Silver Nanoparticles Decorated Graphene Filled PVDF/PMMA Blends with Advanced electrical, mechanical, and thermal properties

Afifeh Khorramshokouh
Hesam Ramezani
Mehdi Sahami
MEHDI SHARIF (sharif@iaushiraz.ac.ir)
Islamic Azad University

Research Article

Keywords: Nanocomposite, PVDF/PMMA blend, Silver nanoparticle, Reduced graphene oxide, Green-synthesis

Posted Date: March 18th, 2022

DOI: https://doi.org/10.21203/rs.3.rs-1455192/v1

Abstract

In this paper, silver nanoparticles decorated reduced graphene oxide (rGO-Ag) nanohybrids were prepared using an environmentally-friendly approach and incorporated as reinforcement in poly(vinylidene fluoride)-poly(methyl methacrylate) blends via melt mixing process. The effect of rGO-Ag nanohybrids was studied on various properties of the blends using different characterization methods. Fourier transform infrared (FTIR), X-ray diffraction (XRD), and transmission electron microscopy (TEM) results confirmed the successful synthesis of rGO-Ag nanohybrids. The mechanical, electrical, and thermal properties of the resulting rGO-Ag filled nanocomposites were investigated using tensile, thermogravimetric analysis (TGA), and impedance spectroscopy methods. The Halpin-Tsai model also adjusted for PVDF/PMMA/rGO-Ag composites and the results confirmed that this model works well for the prediction of the tensile modulus. Investigation of mechanical properties demonstrated that the presence of rGO-Ag nanohybrids increased the yield strength and elastic modulus of the samples with the addition of only 1 wt % to the chosen blend sample. Impedance spectroscopy test results showed that the addition of rGO-Ag nanohybrids to PVDF/PMMA blend can effectively enhance the conductivity of the blends. Finally, TGA results demonstrated that the addition of rGO-Ag nanohybrids affected the thermal behavior of the samples and increased the thermal stability and degradation temperature of the resulting nanocomposites compared to the base PVDF/PMMA blend.

1. Introduction

In recent years with respect to the advances in technology and science, the need for new materials with special properties is more than ever. In this regard, polymer nanocomposites, due to their lightweight, low cost, recyclability, high mechanical properties, and compatibility with the environment, are facing great demands in various industries compared with metallic compounds and ceramics. One of the main shortcomings of polymers is that most of them cannot be used alone and should be modified. The main methods for modification of polymers include blending, grafting, and coating [1–7]. Blending is the most preferred method due to relative ease of process and cost-effectiveness, and can also enhance the properties of polymer materials. Blending has also three methods which include melt blending, solution blending, and in situ polymerization blending [1–3, 8]. In order to blend polymers with each other, they should be compatible and the microstructure of the resulting blend is determined by the blending method and polymer matrices.

Fluoropolymers are one of the best protective materials and they are often used as protective films or coatings [7]. PVDF is a fluoropolymer with good thermal stability, mechanical properties, resistance to chemical substances, oxidation, and UV irradiation as well as a fantastic appearance. PVDF is also one of the few semi-crystalline polymers having three crystalline phases α, β, and γ phases [1]. The main disadvantage of PVDF is its high price, thus it is often mixed with other polymers to solve this problem [6, 7, 9]. One of the polymers that has good compatibility with PVDF and can be blended with it is poly(methyl methacrylate) (PMMA). PMMA can effectively lower the cost and also improve the adhesion properties of PVDF and is often chosen to blend with it [10, 11]. PMMA is an amorphous polymer and has

high rigidity, transparency, and chemical resistance which is widely used in various applications [12]. The miscibility and compatibility of PVDF and PMMA have been extensively studied in many studies. These two polymers have proved to be compatible in a wide range of compositions in solid state and they are completely miscible in the molten state [13–15]. The main reason for this miscibility is the intermolecular interactions between carbonyl groups of PMMA and the CH2 and CF2 groups of PMMA. These interactions include dipolar interactions and hydrogen bondings, respectively. Studies also showed that the blending of PVDF with PMMA results in a transfer in crystallization from α phase to β phase which is thermodynamically unstable in the pure form of PVDF [7, 16, 17]. Another method to improve the properties of polymers is to add fillers to their matrix, hence, there is much interest in the investigation of various combinations of polymers and fillers [18, 19]. It has been reported that by the addition of small amounts of nanohybrids to polymer matrices a significant improvement in their physical properties was observed. Carbon nanotubes (CNT) and nanoclays which are one and two-dimensional fillers are widely studied in recent years [1–3]. In addition, graphene and its derivatives (e.g. graphene oxide (GO) and reduced graphene oxide (rGO)) have attracted much interest in recent years due to their exceptional properties, and the incorporation of these fillers in the polymer matrices has led to significant improvements [4, 9]. Reduced graphene oxide is the oxidized form of graphene with relatively lower functional groups in comparison with GO which can solve the dispersion problem of graphene sheets. As a result of the existence of carbonyl, carboxyl, and hydroxyl groups on its surface, rGO can be dispersed in polar solvents and also facilitate the formation of interactions with the matrices possessing the same functional groups through strong hydrogen bonds [20]. As a result of the extraordinary mechanical, thermal, and optical properties of rGO alongside its ease of dispersion in many solvents and matrices which is due to the presence of oxygen-containing functional groups, it has been used as a reinforcing filler to enhance different properties of PVDF, PMMA, and PVDF/PMMA blends [21–23]. Although rGO is an electrical conductor, because of the availability of oxygen-containing groups on its surface its conductivity properties can be further enhanced to be used for electrical applications. In order to increase the conductivity of different materials, one-dimensional metals such as Ag, Cu, and Au can be good choices [24–26]. By the incorporation of these metals which have unique properties into polymer matrices, new composites with desirable properties can be produced. One of the best metal particles for enhancing the electrical properties of rGO is silver nanoparticles and the resulting product is known as rGO-Ag nanohybrid. These nanohybrids have been used in many studies to add electrical conductivity, mechanical enhancement, thermal stability, and also antibacterial and antifouling properties [22, 27, 28].

In this study, rGO-Ag nanohybrids were synthesized by the reduction of silver ions on the rGO surface using ascorbic acid as a reducing agent. Synthesis was carried out in an aqueous solution, which is a versatile, low-cost, and environmentally friendly process. These nanohybrids could be easily dispersed into water or common organic solvents to form a stable suspension without any additional protection by polymeric or surfactant stabilizers. Since rGO-Ag nanohybrids possess very good electrical, mechanical, and thermal properties, they can be used to enhance the properties of PVDF/PMMA blends. Thus, the main goal of this study is to prepare a PVDF/PMMA nanocomposite containing silver nanoparticles

decorated rGO nanosheets and an investigation of its properties which was not carried out in past studies.

2. Experimental

2.1 Materials

PVDF (solid spot D 140, M_w= 20 kg/mol), PMMA (Sigma Aldrich, M_w= 95 kg/mol), graphite powder (≤20 µm, 99.9%), sodium nitrate (Sigma Aldrich), potassium permanganate (Sigma Aldrich), sulfuric acid (Sigma Aldrich), silver nitrate (Sigma Aldrich, 169 kg/mol), ascorbic acid (Sigma Aldrich). The GO nanosheets were synthesized using the modified Hummers method according to a previous study by Ramezani et. al [20]. Afterward, GO nanosheets were reduced using ascorbic acid to obtain rGO.

2.2 Graphene oxide synthesis

The modified hummers method was employed to synthesize GO by oxidizing natural graphite [5]. The procedure consists of several oxidation stages, 1 g natural graphite powder was added to a mixture of 46 mL H_2SO_4 and 1 g $NaNO_3$ inside a flask with constant stirring and placed in an ice bath to keep the temperature under 5 ˚C. Afterward, 6 g $KMnO_4$ Was gradually added and stirred for one hour while the temperature was under control. In the next step, the ice bath was removed and the temperature was increased to 35˚C while stirring the mixture for 1 h. Then, 92 mL distilled water was added to the mixture and the temperature was increased to 95˚C and kept at the same temperature for 0.5 h, and then the temperature was lowered and 150 mL distilled water was added to dilute the mixture followed by 10 mL H_2O_2 (30 wt. %). The mixture was centrifuged and the resulting solid which is GO sheets were washed with HCl solution (5 wt. %) and distilled water to remove metal ions and reach a neutral pH. Finally, GO sheets were dried in an oven and dispersed in water.

2.3 Green Synthesis of rGO-Ag Nanohybrids

In order to prepare rGO-Ag nanohybrids, 0.8 g of GO powder was dispersed in 40 ml distilled water using ultrasonication for 1 h, and then the stabilized GO colloid was transferred to a 500 ml flask containing a solution of distilled water and silver nitrate (4 g $AgNO_3$ in 40 ml distilled water) and 1.76 ml of ascorbic acid which was dissolved in 30 ml distilled water was gradually added to the solution to extract Ag ions from $AgNO_3$ and reduce oxygen-containing groups of GO. The mixture was then stirred for 2 h. Finally, rGO-Ag nanohybrids were separated from the solution and dried in a vacuum oven for 24 h at 85°C.

2.4 Preparation of the PVDF/PMMA/rGO-Ag Nanocomposites

Polymer nanocomposites were prepared by melt mixing method using an internal mixer at 180ºc and 60 rpm. The concentration and nomenclature of each component are presented in Table 1.

Table 1. Composition and codes of the prepared samples

	Composition (%)		
sample	PVDF	PMMA	GO-Ag
PVDF	100	0	0
PV 0.8	80	20	0
PV 0.7	70	30	0
PV 0.6	60	40	0
PV/PM	50	50	0
PM 0.6	40	60	0
PM 0.7	30	70	0
PM 0.8	20	80	0
PMMA	0	100	0
PM 0.8/rGO-Ag 0.5	20	80	0.5
PM 0.8/rGO-Ag 1	20	80	1
PM 0.8/rGO-Ag 1.5	20	80	1.5

2.5 Characterization

2.5.1 X-Ray Diffraction (XRD)

The X-Ray Diffraction (XRD) analysis was carried out using D8advance diffractometer at a rate of 0.05 deg/min from $2\theta = 10^{\circ}$ to $2\theta = 70^{\circ}$.

2.5.2 Fourier Transform Infrared Spectroscopy (FTIR)

Fourier Transform Infrared (FTIR) spectra was performed using D8advance spectrometer by incorporating the samples in the KBr disk.

2.5.3 Impedance spectroscopy

Electrical properties of samples were measured using D8advance machine at a frequency rate of 20-20000 HZ.

2.5.4 Scanning Electron Microscopy (SEM)

Scanning electron microscopy (SEM) was performed using a Hitachi-S-4500 microscope. The images were taken from the fracture surface of the test specimens that were broken inside liquid nitrogen.

2.5.5 Transmission Electron Microscopy (TEM)

The TEM analysis of Ag–rGO was performed by the JEOL 2100 instrument. A small amount of the sample was dispersed in acetone through sonication and a drop of this dispersed solution was put on the copper grid for HRTEM analysis.

2.5.6 Tensile Test

The mechanical properties were measured according to ASTM-D360 using Instron 4301 universal mechanical tester at a rate of 1.2 mm/min.

2.5.7 Thermogravimetry Analysis

Thermogravimetric analysis (TGA) was carried out by TA Instruments SDT Q600 to investigate the thermal properties of the samples. The test was carried out under a nitrogen atmosphere and by a heating rate of 10 ºC per minute.

3. Results And Discussion

3.1 Characterization of GO nanosheets and rGO-Ag nanohybrids

3.1.1 FTIR spectroscopy

Figure 1 represents the FTIR spectroscopy for GO nanosheets and rGO-Ag nanohybrids to investigate the successful synthesis of these nanofillers. Starting with the GO nanosheets, multiple peaks can be observed at 1720, 1618, 1400, 1260, 1132, and 1049 cm^{-1}. These peaks are related to oxygen-containing groups that exist on the surface of the GO nanosheets and show the presence of carbonyl and carboxyl groups, C-O-H functionality, breathing vibrations of epoxide group, and C-O stretching vibrations, respectively [20].

As for the rGO-Ag nanohybrids, the peaks are very similar to those for the GO nanosheets and the wavenumbers are also the same, but the intensity of these peaks experienced a reduction which can be a result of the decoration of GO nanosheets with silver particles. This observation confirms that GO nanosheets are successfully decorated with silver particles and it is in accordance with previous studies [10, 27, 28]. In addition, the peak in 1387 cm^{-1} which is associated with the in-place deformation of O-H bonds in hydroxyl groups for GO disappeared in FTIR spectra of rGO-Ag and it is the result of the reduction of GO with ascorbic acid [11].

3.1.2 XRD

The XRD patterns of GO nanosheets and rGO-Ag nanohybrids are presented in Fig. 2. The peak at $2\theta = 10.13^{\circ}$ shows that graphite was oxidized well and GO nanosheets were synthesized successfully. The main peak in the XRD pattern of GO at $2\theta = 10.13^{\circ}$ is disappeared in the XRD pattern of rGO-Ag nanohybrids and this indicates that ascorbic acid has reduced oxygen-containing groups of GO nanosheets to a high extent [29]. Apart from that, the higher intensity of the characteristic peaks related to

the Ag part of the nanohybrids compared with GO implies that Ag nanoparticles facilitated the exfoliation of rGO nanosheets which also leads to the disappearance of the peak at 2θ = 10.13˚ [28].

The XRD profile of rGO-Ag nanohybrids has four peaks at 2θ = 38.3°, 44.4°, 64.6°, and 77.4°, which correspond to the (111), (200), (220), and (311) crystallographic planes, respectively. This confirms the presence of silver nanoparticles on the surface of GO nanosheets and is in good agreement with the results reported in the literature [11].

3.1.3 TEM Images

The TEM image of rGO-Ag nanohybrids is presented in Fig. 3. As shown in this figure, the crumpled and wrinkled surface of rGO stacked together to form a multilayer structure that embraces the Ag nanoparticles and modifies their surface energy which is the main reason for the agglomeration of Ag nanoparticles. Furthermore, because of the different extent of reduction in various rGO nanosheets, Ag nanoparticles have to compete with each other to attach to the surface of rGO nanosheets which have more oxygen-containing groups on their surface. This means that those nanosheets which had been reduced more can interact with less Ag^+ ions because of the limited OH^- ions available on their surface. Hence Ag^+ ions tend to interact with nanosheets with more OH^- ions available [30].

3.1.4 Mechanical properties of PVDF/PMMA blends

Mechanical properties are the most important factor when it comes to application and many polymers are being chosen to be used in different applications because of their superior mechanical properties. Thus, to find out the best blend composition to be reinforced with the nanohybrids, the mechanical properties of every sample were measured and compared together in Figs. 4, 5, and 6. Samples with PVDF as their matrix showed a downtrend in yield strength as the PMMA content increased up to 40 wt%, after this turning point yield, strength is directly related to the PMMA content because it is the new matrix and has better mechanical properties than PVDF. According to Fig. 4, PM 0.8 sample has the highest yield strength (62 MPa) which can be due to the superior mechanical properties of PMMA and also the possible changes in the crystalline structure of the samples [31].

As for the elongation at break, results showed that by increasing the PMMA content, the elongation at break of the samples decreases because of the nature of PMMA which has a low tensile strain. It can be observed that for the PV 0.8 sample, elongation at break increases which can be due to the addition of PMMA and the lower crystallinity and formation of the β crystalline phase in PVDF but this trend changes as soon as the PMMA content starts to rise [32]. At this point, the mechanical properties of the blend will be attributed to the high strength and the low tensile strain of the glassy phase. It is to be noted that the strong interactions between PVDF and PMMA chains lead to the enhancement of mechanical properties of the nanocomposites [24, 25].

Elastic modulus does not follow a specific trend and varies with the composition but as PMMA becomes the dominant phase, a certain uptrend can be recognized which climaxes at 1.945 GPa for PM 0.8. Once

again this increase is the result of the superior mechanical properties of PMMA which has a high elastic modulus compared to PVDF.

Finally, results showed that PM 0.8 possesses the best mechanical properties and the potential to be used in applications that require desirable yield strength and elastic modulus. Consequently, PM 0.8 was chosen to be reinforced with 0.5, 1, and 1.5 wt % of rGO-Ag nanohybrids. For the next stage, the resulting nanocomposites were put to various tests to find out their mechanical, thermal, electrical, and morphological properties.

3.2 Characterization of PVDF/PMMA/rGO-Ag nanocomposites

3.2.1 Mechanical properties

Tensile strength, elongation at break, and elastic modulus of the PM 0.8/rGO-Ag 0.5, PM 0.8/rGO-Ag 1, and PM 0.8/rGO-Ag 1.5 are presented in Figs. 7, 8, and 9. It can be observed that tensile strength and elastic modulus experienced an improvement with the increase of rGO-Ag nanohybrids while elongation at break of the samples decreased. In addition to that, PM 0.8/rGO-Ag 1 sample has shown the highest yield strength and elastic modulus compared to other nanocomposites with 80 MPa and 2.453 GPa, respectively.

This can be attributed to the presence of strong interactions between the oxygen-containing groups on the surface of rGO nanosheets and the CF_2 segments of PVDF and also the presence of Ag nanoparticles on the surface of rGO nanosheets which facilitates the stress transfer between the matrix and rGO nanosheets through the interactions between Ag and matrix, and also Ag and rGO nanosheets [33–35].

As for the PM 0.8/rGO-Ag 1.5 sample, although it has a superior yield strength and elastic modulus to PM 0.8 and PM 0.8/rGO-Ag 0.5 samples; it is still unable to compete with PM 0.8/rGO-Ag 1 which can be mainly due to the agglomeration of the nanohybrids inside the polymer matrix. Silver nanoparticles are known for having a high tendency to form agglomerates inside many polymer matrices to minimize their surface energy. Hence, rGO nanosheets are used to hold these nanoparticles in place and prevent them from forming agglomerates. By the addition of 1.5 wt % of the nanohybrids and as a result of the increase in silver content inside the matrix it can be presumed that silver particles had the chance to form agglomerates and make a negative impact on the mechanical properties of the nanocomposite [10, 36, 37].

3.2.2 Halpin -Tsai model

One of the most widely used models for the prediction of elastic modulus in composites consisting of two phases is the Halpin - Tsai model. Since it can be presumed that the PVDF/PMMA part of the composites acts as an integrated matrix and rGO-Ag nanohybrids disperse inside them, then the Halpin – Tsai model can be used for the prediction of elastic modulus. This model can also help with the determination of the morphology of the matrix and the efficiency of filler dispersion. Halpin - Tsai model

is given by Eq. 1 which was also used in similar calculations by other researchers to predict the properties of binary composites.

$$\frac{E_1}{E} = \frac{(1 + A_i B_i \phi_2)}{(1 - B_i \phi_2)} \quad (1)$$

B_i can be calculated using Eq. 2

$$B_i = \frac{\left(E_1 / E_2\right) - 1}{(E_1 / E_2) + A_i} \quad (2)$$

Subscripts 1 and 2 represent the matrix and the dispersed phases, respectively, and ϕ_2 is the volume fraction of the fillers. As for the constant A_i, it can be determined with respect to the morphological properties of the system. For the dispersed phase consisting of hard materials such as rGO-Ag nanohybrids, A_i is equal to 1.5. In order to use the equations, E_1 and E_2 should also be determined which are the elastic modulus of PM 0.8 and rGO-Ag nanohybrids, respectively. According to Fig. 6, the elastic modulus of PM 0.8 is 1.945 GPa but for the nanohybrids, it was presumed that silver nanoparticles are not able to further increase the modulus of rGO. In addition, they act as conductive interfaces between rGO and the matrix which presumably transfer the loads to their substrate, in other words, rGO. Hence, E_2 was presumed to be the theoretical value for the elastic modulus of rGO which is approximately 325 GPa. The results of the Halpin – Tsai calculations are presented and compared with experimental elastic modulus values in Fig. 10.

As it is shown in the figure, there is a certain inconsistency between the obtained values from the equation and the experimental data. The reason for the observed difference in PM 0.8/rGO-Ag 1.5 can be related to the fact that the Halpin – Tsai equation does not take the agglomeration of the fillers into account, as a result, it predicts that the modulus should continue to rise with the addition of fillers. However, fillers with planar geometry tend to agglomerate in rather low concentrations which have also happened for samples containing 1.5 wt% of the nanohybrids. The reason for the inconsistency between the results for PM 0.8/rGO-Ag 1 can be attributed to the synergistic effect of the good dispersion of the nanohybrids and the interactions between nanohybrids and the matrix.

3.2.3 Morphological observation

The SEM images were used to investigate the effect of rGO-Ag on the morphology of PMMA/PVDF blends and the results are presented in Fig. 11. As it can be seen in Fig. 11 (a), the two amorphous and semi-crystalline phases of PMMA and PVDF are compatible with each other and they have formed a homogenous system together. Figure 11 (b) shows the fracture surface of the PM 0.8/rGO-Ag 0.5 nanocomposite, it can be observed that the nanohybrids have a good dispersion inside the matrix and no agglomerates are available. Moving on to Fig. 11 (c) which shows the fracture surface of PM 0.8/rGO-Ag 1 nanocomposite, it is observed that rGO-Ag nanohybrids are uniformly distributed with the least agglomerations in the polymer matrix. It is due to the effective interactions between oxygen-containing

functional groups on the rGO surface and CF_2 segments in PVDF and also the strong interactions between the rGO nanosheets and PMMA functional groups [4, 16]. Finally, Fig. 11 (d) demonstrates the PM 0.8/rGO-Ag 1.5 nanocomposite which has some agglomerations at its fracture surface that can lead to problems in stress transfer between the matrix and rGO nanosheets. In addition, Fig. 11 (d) also shows that many rGO-Ag nanohybrids are not agglomerated and have a good dispersion inside the matrix which can explain the improved mechanical properties of PM 0.8/rGO-Ag 1.5 nanocomposite although it has some agglomerations.

3.2.4 Impedance spectroscopy

Figure 12 shows the ac conductivity of the PM 0.8 and PMMA/PVDF nanocomposites as a function of frequency. As it can be seen, PM 0.8 shows an almost linear response to the increase of the frequency which is the characteristic behavior of non-conductive materials. In contrast, the nanocomposite samples act almost independently towards the frequency change at low frequencies as the nanohybrids content rises. This observation proves that by the addition of the nanohybrids, ac conductivity properties are added to the nanocomposites. In addition to that, the ac conductivity graph of the nanocomposites containing 0.5 and 1 wt % of the nanohybrids are quite the same which shows that 0.5 wt % can be the percolation threshold which is lower than most of the similar previous studies [38, 39]. This implies that rGO-Ag nanohybrids have superior electrical properties due to the synergy between the electrical properties of silver particles and rGO nanosheets and also their strong interactions. On top of that, this can be presumed that apart from the reduction at the nanohybrids production stage, some oxygen-containing groups were reduced during the mixing stage and hot press molding as a result of the high processing temperature. This reduction leads to an increase in the electrical properties of rGO nanosheets [4, 40].

The highest ac conductivity and the most independent response to frequency change belong to PM 0.8/rGO-Ag 1.5 sample. This observation can be due to the presence of more rGO-Ag nanohybrids which act as conductive bridges to facilitate the electron transfer in nanocomposites [26].

3.2.1 Thermogravimetric analysis.

Thermal behavior and stability of PM 0.8 and nanocomposite samples were determined using thermogravimetric analysis and test results are shown in Fig. 12. As shown in the figure, the general thermal profiles of all the samples are quite the same and consist of two stages. These stages are related to the degradation of PVDF and PMMA contents of the samples. By the introduction of rGO-Ag nanohybrids, both of the degradation stages occur at higher temperatures which can be attributed to the thermal stability of Ag nanoparticles and rGO nanosheets. The PM 0.8/rGO-Ag sample has the highest thermal stability and the lowest degradation that can be related to the better dispersion of nanohybrids inside the nanocomposite and also higher density of interactions between the matrix and nanohybrids [29, 41]. The PMMA portion of the samples started to degrade at around 360 ºC for PM 0.8 sample and increased to a maximum of 375 ºC for the PM 0.8/rGO-Ag 1 nanocomposite. Apart from that, the PVDF part of the samples started the thermal degradation at 462 ºC for the PM 0.8 sample and reached 480 ºC

for PM 0.8/rGO-Ag 1 nanocomposite. These observations can be the result of retarding the chain scission of C-F and C-H bonds of the PVDF through providing a thermal shield by the nanohybrids and also trapping the free radicals that are produced in the system. Thus, thermal stability and degradation temperature increase with the addition of nanohybrids into the system [41].

4. Conclusion

Silver nanoparticles decorated reduced graphene oxide nanohybrids (rGO-Ag) were prepared using an environmentally-friendly approach and incorporated in poly(vinylidene fluoride)-poly(methyl methacrylate) blends via melt mixing process to study their effect on the structure and properties of the blends. Results demonstrated that by the addition of low wt. % of the nanohybrids to the blends, the resulting nanocomposites show enhanced mechanical, thermal, and electrical properties. These enhanced properties demonstrate that rGO-Ag nanohybrids can be considered as reinforcing fillers that can add different properties to PVDF/PMMA blends to facilitate the use of these polymers in various applications. These nanohybrids can also be used to introduce antibacterial and biofouling properties in different matrices, which is another possible field of study for these promising reinforcing fillers.

Declarations

6.1 Funding

The authors declare that no funds, grants, or other support were received during the preparation of this manuscript.

6.2 Competing Interests

All authors contributed to the study's conception and design. Material preparation, data collection, and analysis were performed by Afifeh Khorramshokouh, Hesam Ramezani, Mehdi Sahami, and Mehdi Sharif. The first draft of the manuscript was written by Afifeh Khorramshokouh and all authors commented on previous versions of the manuscript. All authors read and approved the final manuscript.

6.3 Data Availability Statement

The raw/processed data required to reproduce these findings cannot be shared at this time as the data also forms part of an ongoing study.

References

1. R.R. Abbas, N. Rammo, E.A. Al-Ajaj, Structure and piezoelectricity in blends of PVDF films PVDF. J. kerbala Univ. **6**(4), 201–208 (2008)
2. T. Hosoda, T. Yamada, *Effect of TiO2 on morphology and mechanical properties of PVDF/PMMA blend films prepared by melt casting process*. Journal of Applied Polymer Science, 131(13). 2014

3. S. Ansari, E.P. Giannelis, Functionalized graphene sheet—Poly (vinylidene fluoride) conductive nanocomposites. J. Polym. Sci., Part B: Polym. Phys. **47**(9), 888–897 (2009)
4. F. Liu, R. Huo, X. Huang, Q. Lei, P. Jiang, Crystalline properties, dielectric response and thermal stability of in-situ reduced graphene oxide/poly (vinylidene fluoride) nanocomposites. IEEE Trans. Dielectr. Electr. Insul. **21**(4), 1446–1454 (2014)
5. W.S. Hummers Jr., R.E. Offeman, Preparation of graphitic oxide. J. Am. Chem. Soc. **80**(6), 1339–1339 (1958)
6. H. Ramezani, M. Sharif, A. Khorram Shokooh, Graphene-Based Polym. Nanocomposites Basparesh **4**(4), 86–107 (2015)
7. M. Sharma, K. Sharma, S. Bose, Segmental relaxations and crystallization-induced phase separation in PVDF/PMMA blends in the presence of surface-functionalized multiwall carbon nanotubes. J. Phys. Chem. B **117**(28), 8589–8602 (2013)
8. D.R. Dreyer, A.D. Todd, C.W. Bielawski, Harnessing the chemistry of graphene oxide. Chem. Soc. Rev. **43**(15), 5288–5301 (2014)
9. T.D. Dao, H. Lee, H.M. Jeong, Alumina-coated graphene nanosheet and its composite of acrylic rubber. J. Colloid Interface Sci. **416**, 38–43 (2014)
10. W. Shao, X. Liu, H. Min, G. Dong, Q. Feng, S. Zuo, Preparation, characterization, and antibacterial activity of silver nanoparticle-decorated graphene oxide nanocomposite. ACS Appl. Mater. Interfaces **7**(12), 6966–6973 (2015)
11. R.A. Dar, N.G. Khare, D.P. Cole, S.P. Karna, A.K. Srivastava, Green synthesis of a silver nanoparticle–graphene oxide composite and its application for As (III) detection. RSC Adv. **4**(28), 14432–14440 (2014)
12. D. Wang, Y. Bao, J.-W. Zha, J. Zhao, Z.-M. Dang, G.-H. Hu, Improved dielectric properties of nanocomposites based on poly (vinylidene fluoride) and poly (vinyl alcohol)-functionalized graphene. ACS Appl. Mater. Interfaces **4**(11), 6273–6279 (2012)
13. M. Sachin, R. Haridass, B. Ramanujam, *Polyvinylidene fluoride (PVDF)-poly (methyl methacrylate) (PMMA)-expanded graphite (ExGr) conducting polymer blends: Analysis of electrical and thermal behavior.* Materials Today: Proceedings, **28**: p. 103–107. 2020
14. R. Sagar, M. Gaur, V. Kushwah, A. Rathore, D. Piliptsou, A. Rogachev, *Preparation, characterization and microhardness measurements of hybrid nanocomposites based on PMMA + P (VDF–TrFE) and graphene oxide.* Polymer Bulletin: p. 1–22. 2020
15. V.R. Jeedi, E.L. Narsaiah, M. Yalla, R. Swarnalatha, S.N. Reddy, A.S. Chary, Structural and electrical studies of PMMA and PVdF based blend polymer electrolyte. SN Appl. Sci. **2**(12), 1–10 (2020)
16. I. Elashmawi, N. Hakeem, Effect of PMMA addition on characterization and morphology of PVDF. Polym. Eng. Sci. **48**(5), 895–901 (2008)
17. X. Zhao, J. Cheng, J. Zhang, S. Chen, X. Wang, Crystallization behavior of PVDF/PMMA blends prepared by in situ polymerization from DMF and ethanol. J. Mater. Sci. **47**(8), 3720–3728 (2012)

18. A.A. Issa, M.A. Al-Maadeed, A.S. Luyt, D. Ponnamma, M.K. Hassan, Physico-mechanical, dielectric, and piezoelectric properties of PVDF electrospun mats containing silver nanoparticles. C **3**(4), 30 (2017)
19. D. Uniyal, B. Prasad, K.N. Kumar, S. Chandra, V. Panwar, P. Juneja, V. Agarwal, F.S. Gill, *Impedance characteristics analysis of rGO/polymers (PVDF, PMMA, PTFE) nanocomposite membranes.* Materials Today: Proceedings, **26**: p. 320–323. 2020
20. H. Ramezani, T. Behzad, R. Bagheri, Synergistic effect of graphene oxide nanoplatelets and cellulose nanofibers on mechanical, thermal, and barrier properties of thermoplastic starch. Polym. Adv. Technol. **31**(3), 553–565 (2020)
21. A. Islam, A.N. Khan, M.F. Shakir, K. Islam, Strengthening of β polymorph in PVDF/FLG and PVDF/GO nanocomposites. Mater. Res. Express **7**(1), 015017 (2019)
22. A. Kausar, H. Ilyas, M. Siddiq, Aptitude of graphene oxide–silver in advance polymer nanocomposite: a review. Polym.-Plast. Technol. Eng. **57**(4), 283–301 (2018)
23. J. Yang, Y. Zhang, F. Xue, D. Liu, N. Zhang, T. Huang, Y. Wang, *Structural relaxation and dielectric response of PVDF/PMMA blend in the presence of graphene oxide.* Polymer: p. 123998. 2021
24. S. Mohamadi, N. Sharifi-Sanjani, A. Foyouhi, Evaluation of graphene nanosheets influence on the physical properties of PVDF/PMMA blend. J. Polym. Res. **20**(1), 46 (2013)
25. E.K. Oikonomou, S. Tencé-Girault, P. Gérard, S. Norvez, Swelling of semi-crystalline PVDF by a PMMA-based nanostructured diblock copolymer: Morphology and mechanical properties. Polymer **76**, 89–97 (2015)
26. L. He, S.-C. Tjong, Electrical behavior and positive temperature coefficient effect of graphene/polyvinylidene fluoride composites containing silver nanowires. Nanoscale Res. Lett. **9**(1), 375 (2014)
27. E. Mahmoudi, L.Y. Ng, W.L. Ang, Y.T. Chung, R. Rohani, A.W. Mohammad, Enhancing morphology and separation performance of polyamide 6, 6 membranes by minimal incorporation of silver decorated graphene oxide nanoparticles. Sci. Rep. **9**(1), 1–16 (2019)
28. N.T. Huong, N.M. Dat, D.B. Thinh, T.N.M. Anh, T.H. Quan, P.N.B. Long, H.M. Nam, M.T. Phong, N.H. Hieu, Optimization of the antibacterial activity of silver nanoparticles-decorated graphene oxide nanocomposites. Synth. Met. **268**, 116492 (2020)
29. E.F. Aboelfetoh, A.H. Gemeay, R.G. El-Sharkawy, Effective disposal of methylene blue using green immobilized silver nanoparticles on graphene oxide and reduced graphene oxide sheets through one-pot synthesis. Environ. Monit. Assess. **192**, 1–20 (2020)
30. X.-Z. Tang, X. Li, Z. Cao, J. Yang, H. Wang, X. Pu, Z.-Z. Yu, Synthesis of graphene decorated with silver nanoparticles by simultaneous reduction of graphene oxide and silver ions with glucose. Carbon **59**, 93–99 (2013)
31. H. Song, S. Yang, S. Sun, H. Zhang, Effect of miscibility and crystallization on the mechanical properties and transparency of PVDF/PMMA blends. Polym.-Plast. Technol. Eng. **52**(3), 221–227 (2013)

32. S. Pawde, K. Deshmukh, Investigation of the structural, thermal, mechanical, and optical properties of poly (methyl methacrylate) and poly (vinylidene fluoride) blends. J. Appl. Polym. Sci. **114**(4), 2169–2179 (2009)
33. R.K. Layek, S. Samanta, D.P. Chatterjee, A.K. Nandi, Physical and mechanical properties of poly (methyl methacrylate)-functionalized graphene/poly (vinylidine fluoride) nanocomposites: Piezoelectric β polymorph formation. Polymer **51**(24), 5846–5856 (2010)
34. J. Du, H.M. Cheng, The fabrication, properties, and uses of graphene/polymer composites. Macromol. Chem. Phys. **213**(10-11), 1060–1077 (2012)
35. S.N. Tripathi, P. Saini, D. Gupta, V. Choudhary, Electrical and mechanical properties of PMMA/reduced graphene oxide nanocomposites prepared via in situ polymerization. J. Mater. Sci. **48**(18), 6223–6232 (2013)
36. D. Sahu, N. Sarkar, G. Sahoo, P. Mohapatra, S.K. Swain, *Silver imprinted graphene nanocomposites: synthesisis and morphological study*. Appl. Sci. Adv. Mater. Int, 1(6). 2015
37. A. Soroush, W. Ma, Y. Silvino, M.S. Rahaman, Surface modification of thin film composite forward osmosis membrane by silver-decorated graphene-oxide nanosheets. Environ. Science: Nano **2**(4), 395–405 (2015)
38. F. He, S. Lau, H.L. Chan, J. Fan, High dielectric permittivity and low percolation threshold in nanocomposites based on poly (vinylidene fluoride) and exfoliated graphite nanoplates. Adv. Mater. **21**(6), 710–715 (2009)
39. J. Yu, X. Huang, C. Wu, P. Jiang, Permittivity, thermal conductivity and thermal stability of poly (vinylidene fluoride)/graphene nanocomposites. IEEE Trans. Dielectr. Electr. Insul. **18**(2), 478–484 (2011)
40. Z. Wang, J.K. Nelson, H. Hillborg, S. Zhao, L.S. Schadler, Graphene oxide filled nanocomposite with novel electrical and dielectric properties. Adv. Mater. **24**(23), 3134–3137 (2012)
41. F.-C. Chiu, Y.-J. Chen, Evaluation of thermal, mechanical, and electrical properties of PVDF/GNP binary and PVDF/PMMA/GNP ternary nanocomposites. Compos. Part A: Appl. Sci. Manufac. **68**, 62–71 (2015)

Figures

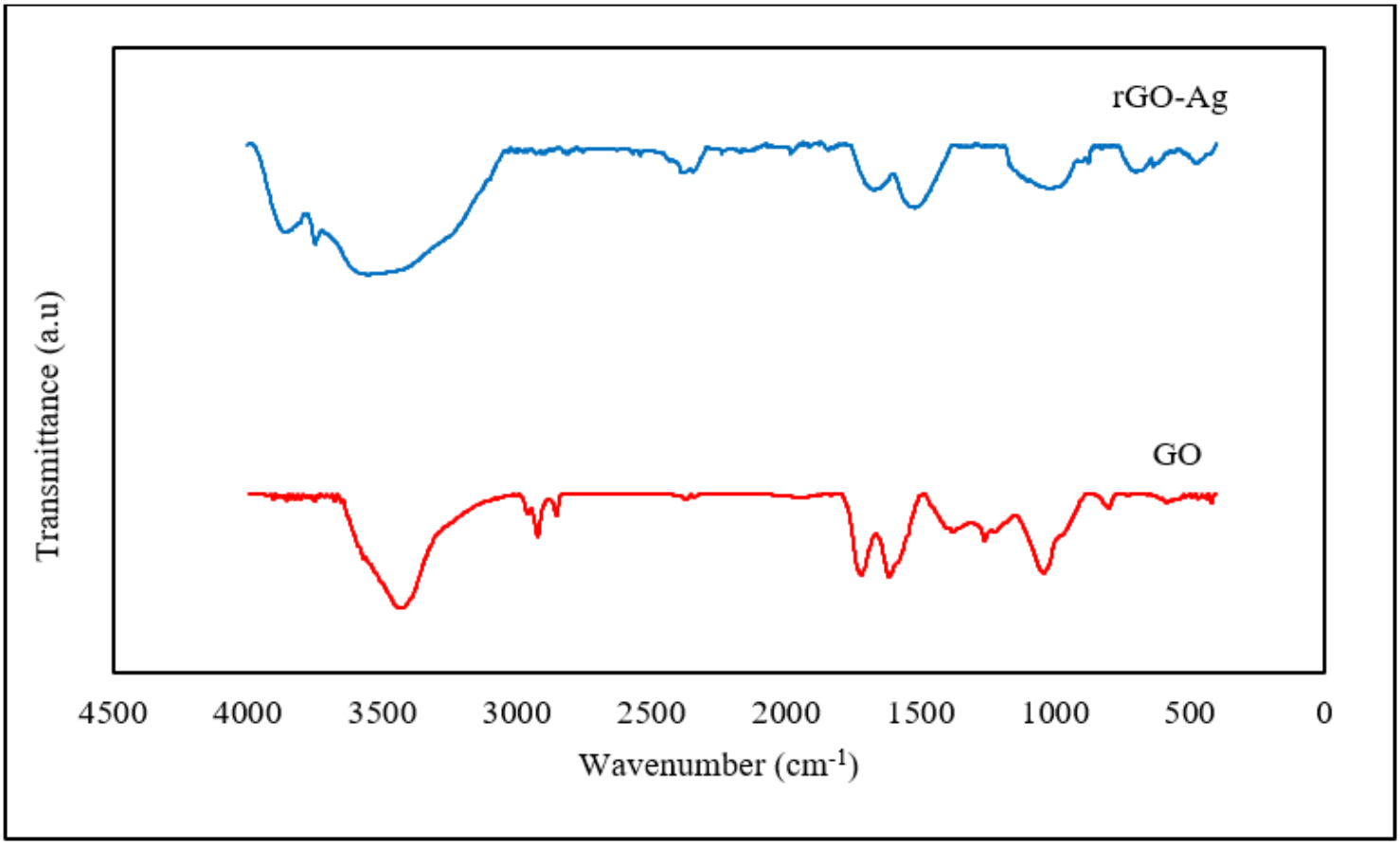

Figure 1

FTIR diffraction of RGO-Ag nanohybrids and GO nanosheets

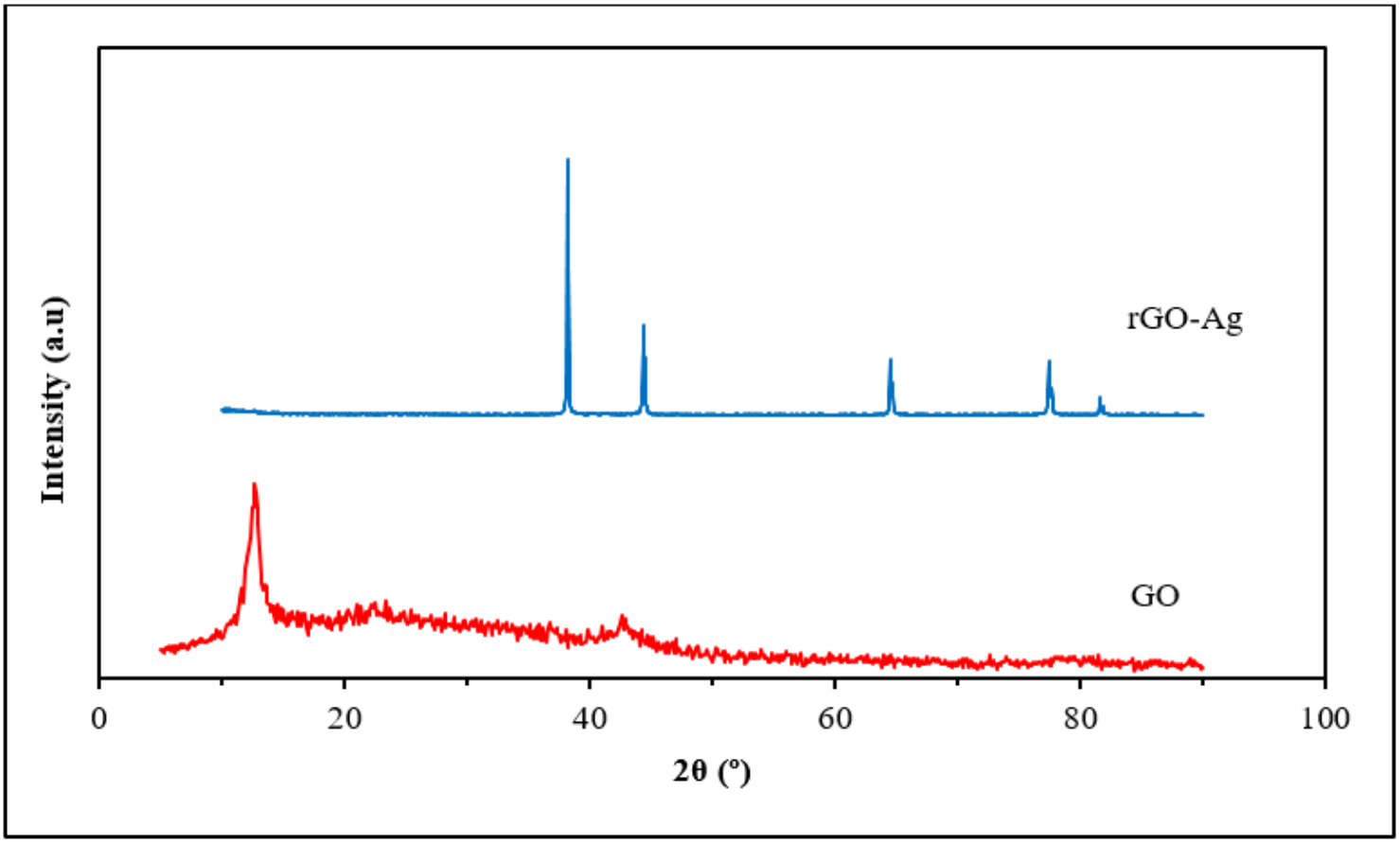

Figure 2

X-ray diffraction of GO nanosheets in comparison with rGO-Ag nanosheets

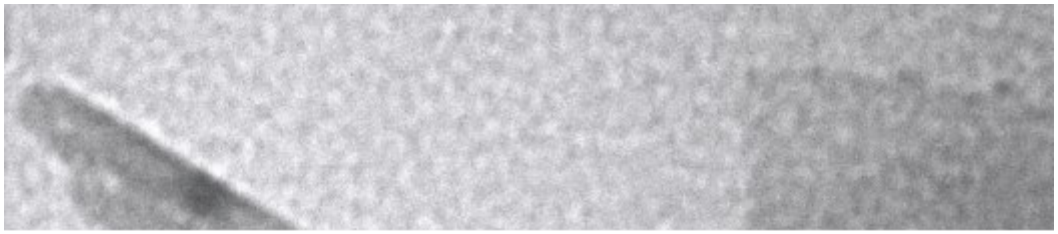

Figure 3

TEM images of rGO-Ag nanohybrids

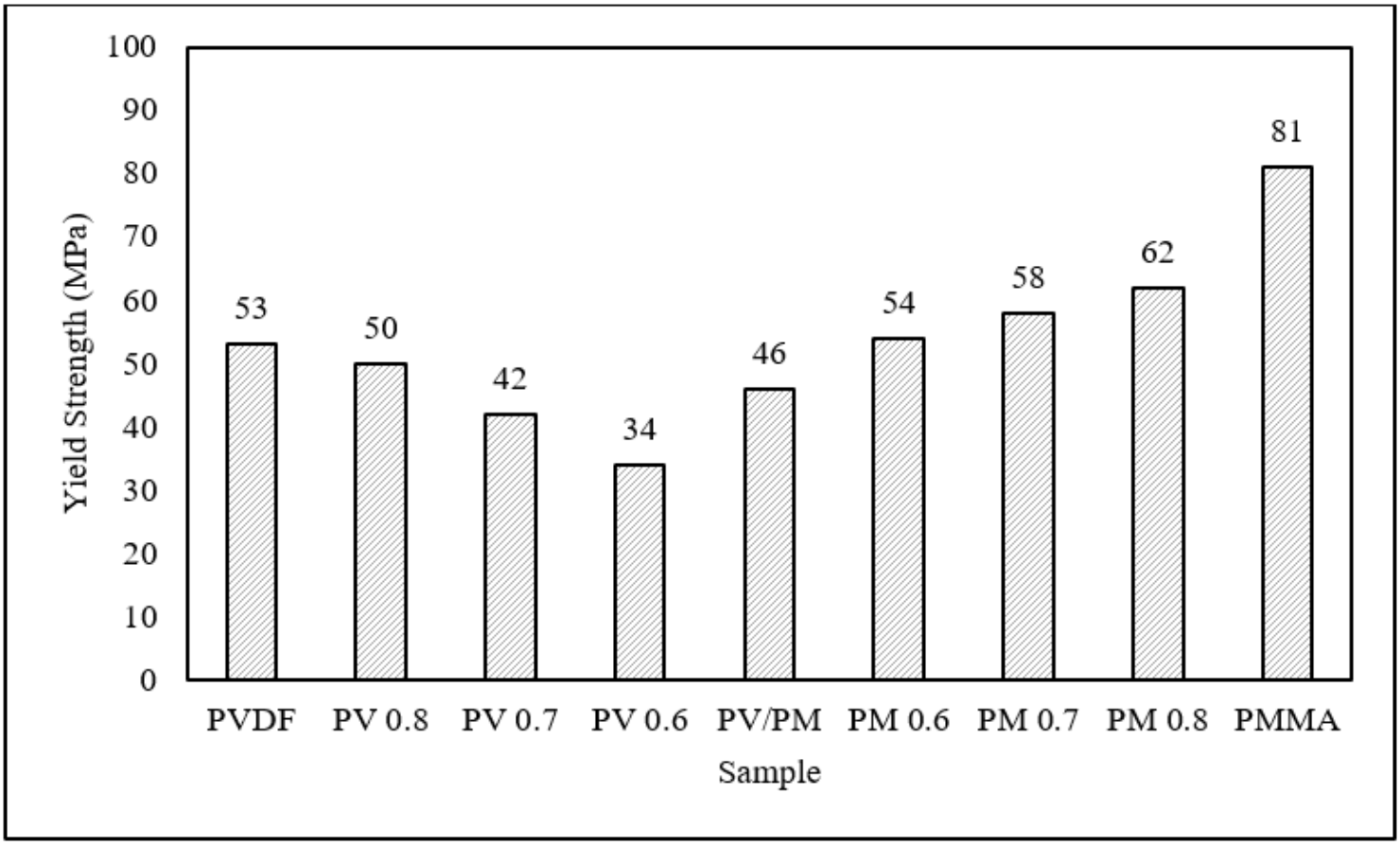

Figure 4

Yield strength of PVDF, PMMA, and PVDF/PMMA blends

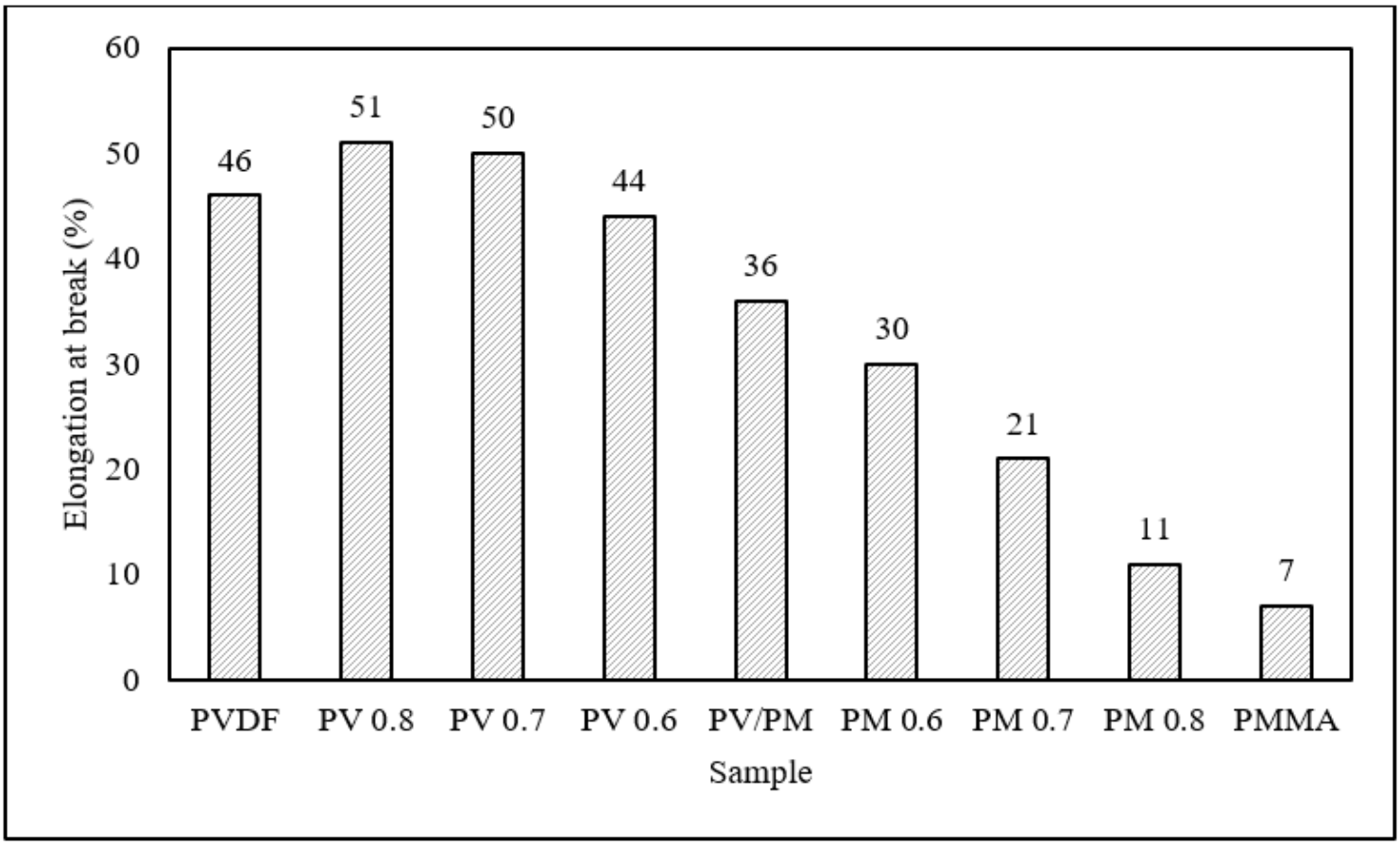

Figure 5

Elongation at break of PVDF, PMMA, and PVDF/PMMA blends

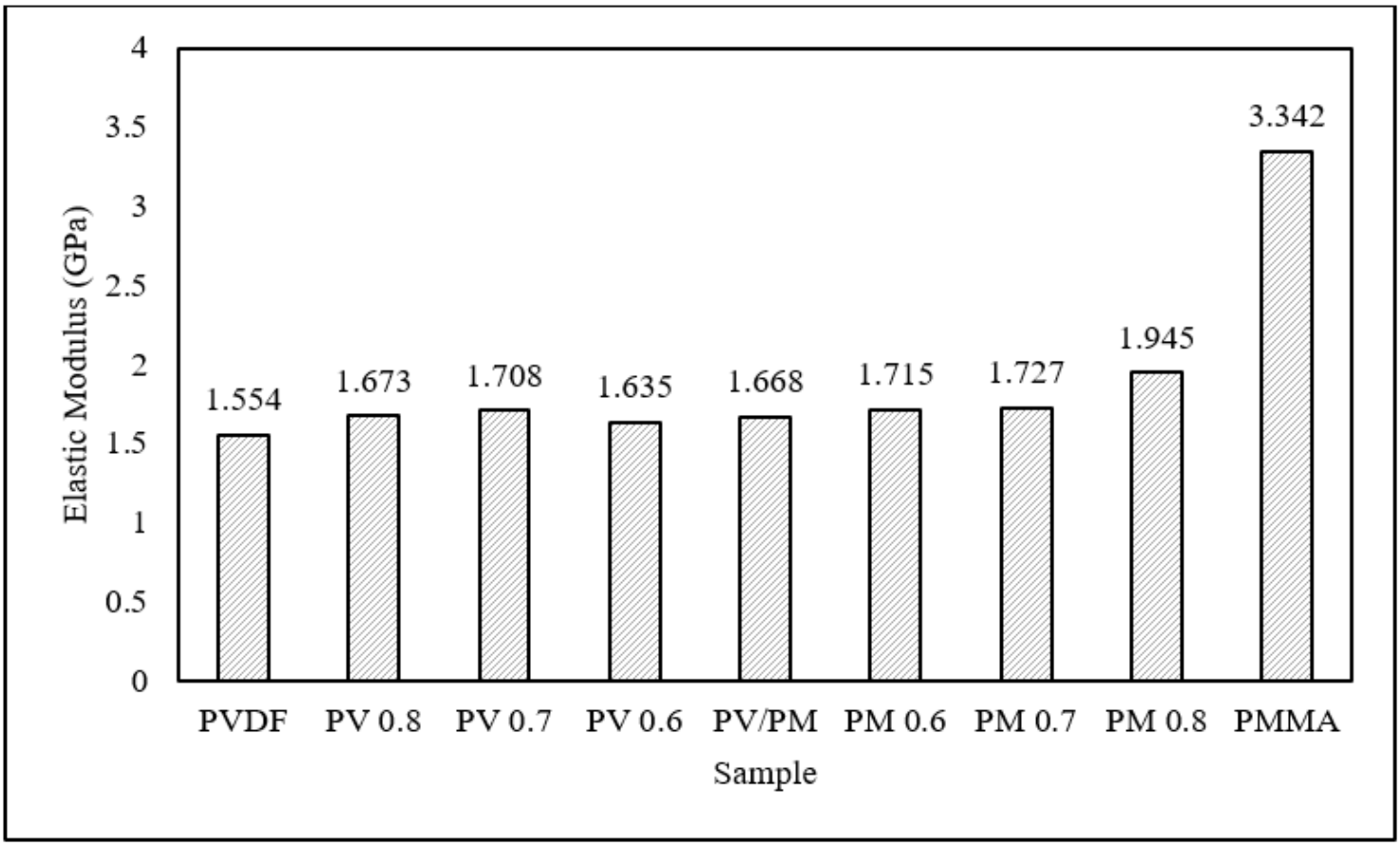

Figure 6

Elastic modulus of PVDF, PMMA, and PVDF/PMMA blends

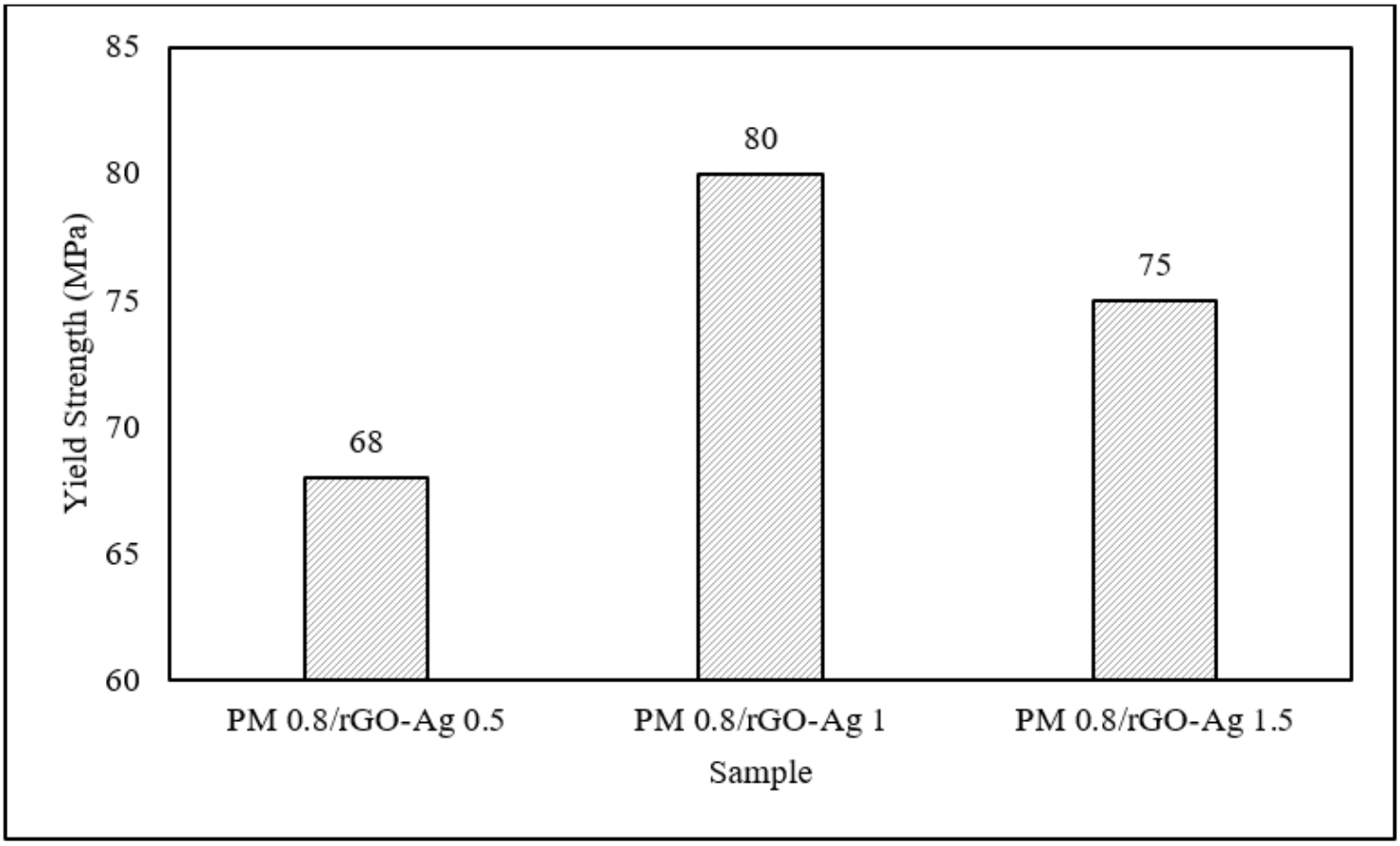

Figure 7

Yield strength of the nanocomposites

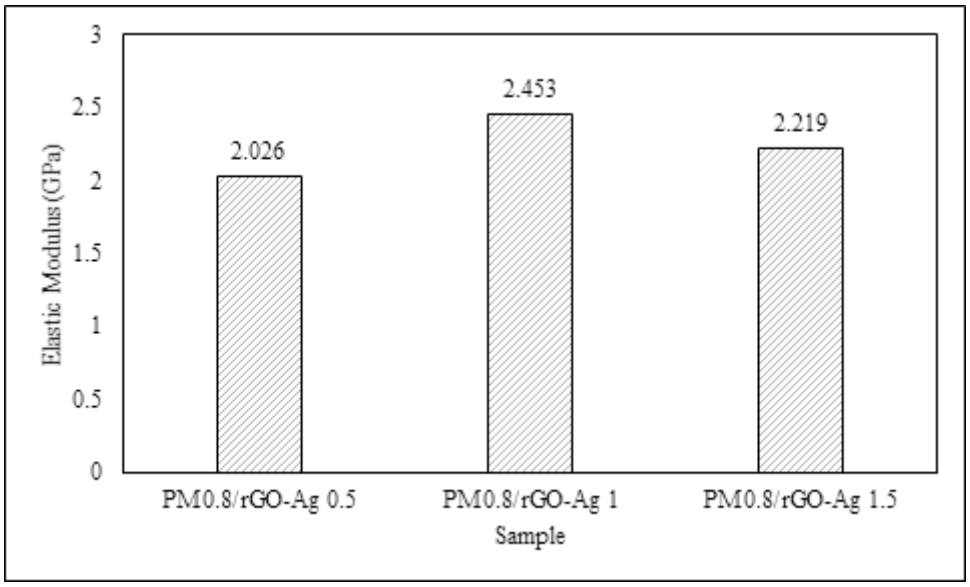

Figure 8

Elongation at break of the nanocomposites

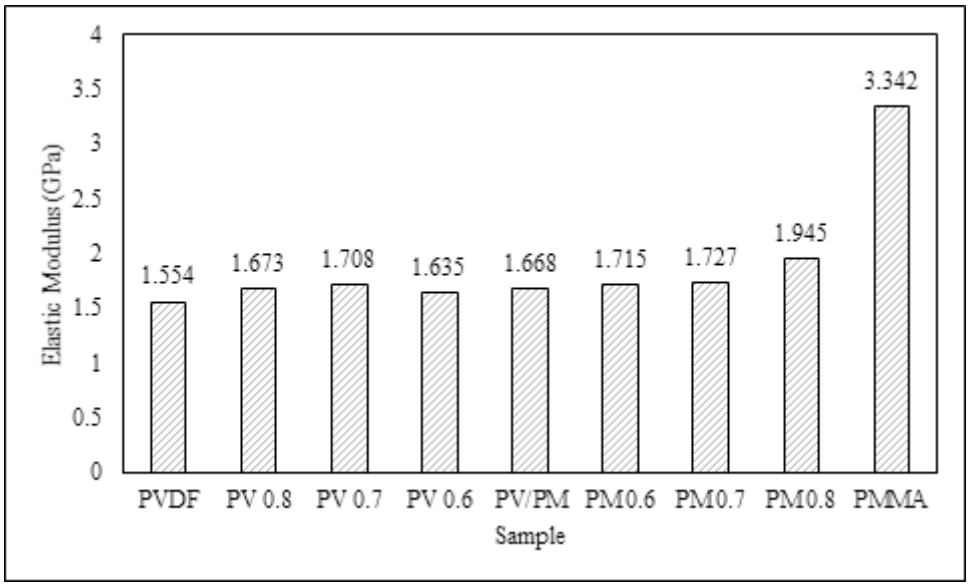

Figure 9

Elastic modulus of the nanocomposites

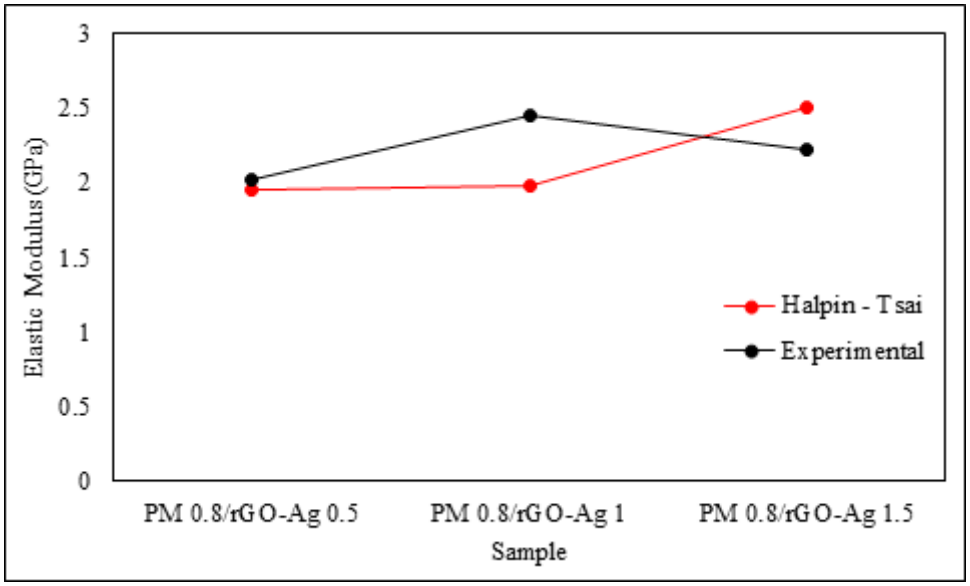

Figure 10

Comparison between the elastic modulus calculated by Halpin – Tsai equation and experimental data

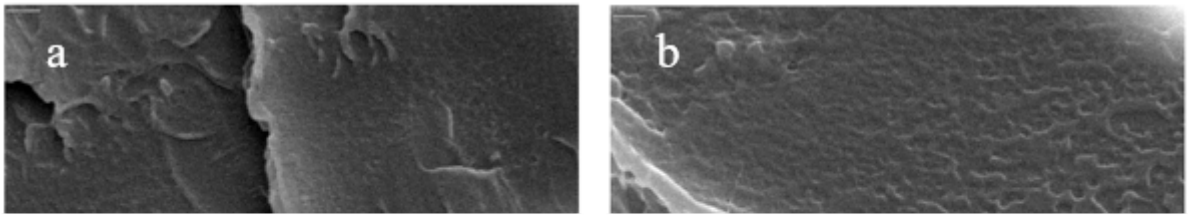

Figure 11

SEM images of a) PM 0.8, b) PM 0.8/rGO-Ag 0.5, c) PM 0.8/rGO-Ag 1, and d) PM 0.8/rGO-Ag 1.5

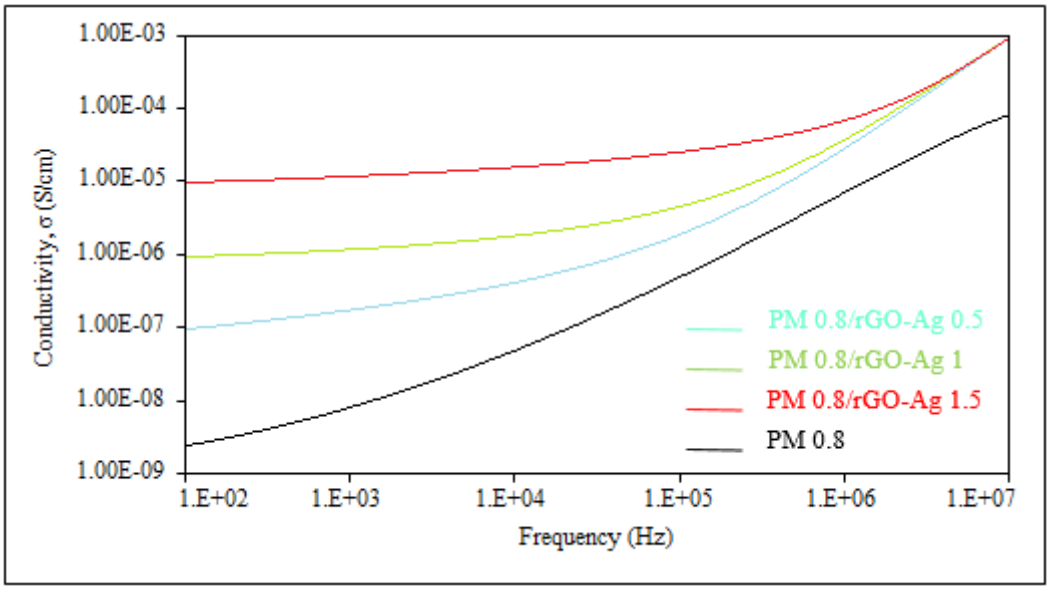

Figure 12

The conductivity of PM 0.8 and the nanocomposite samples

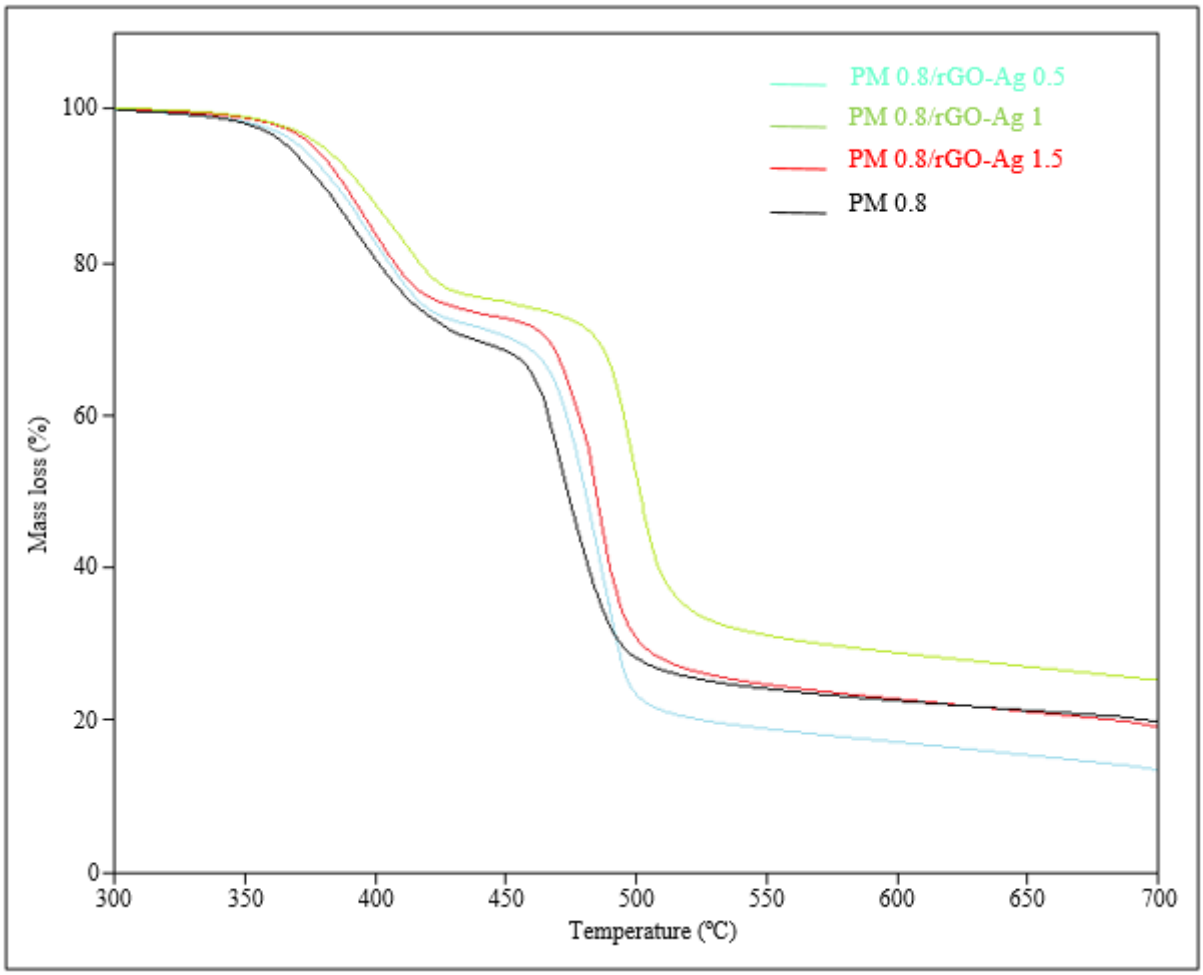

Figure 13

Thermogravimetric analysis of PM 0.8 and nanocomposite samples